Carbon-13 nuclear magnetic resonance in solid ammonium tartrate*

A. Pines, J. J. Chang, and R. G. Griffin†

Department of Chemistry, University of California at Berkeley, Berkeley, California 94720

Inorganic Materials Research Division, Lawrence Berkeley Laboratory, Berkeley, California 94720
(Received 1 April 1974)

Chemical shielding tensors have been determined for ^{13}C in single crystals of ammonium D-tartrate using proton-enhanced NMR. The unit cell contains two molecules, and in some orientations eight lines are resolved from the eight magnetically inequivalent carbon nuclei. Details of the experimental approach, equipment, and analysis are provided, and results are presented for three determinations on two single crystals. These indicate a precision of ± 2 ppm in the determination of the principal values and $\pm 3°$ in the orientation of the principal axes for the carboxyl groups, with lower precision for the hydroxyl groups. The orientations of the principal axes of the tensors are related to the crystallographic (a, b, c^*) axes by employing orientation data from x-ray precession work in this study. The most plausible assignment of the tensors to particular ^{13}C nuclei in the unit cell indicates that the heaviest shielding for ^{13}C in the carboxyl groups occurs when H_0 is perpendicular to the carboxyl plane and the lightest shielding when H_0 is in the carboxyl plane bisecting the C–O bonds. For the hydroxyl ^{13}C, the heaviest shielding occurs with H_0 roughly along the C–O bond. The average principal shielding values are, for the carboxyl ^{13}C, $\sigma_{11}=-110.5$, $\sigma_{22}=-61.7$, $\sigma_{33}=21.6$; and for the hydroxyl ^{13}C, $\sigma_{11}=41.9$, $\sigma_{22}=48.0$, $\sigma_{33}=74.0$ in parts per million (± 2) relative to an external reference of liquid benzene. The effects of hydrogen bonding on the tensors are discussed briefly.

I. INTRODUCTION

Nuclear magnetic resonance of ^{13}C is now accepted as a powerful tool for the study of structure and dynamics in liquids.[1] The advantages of observing ^{13}C rather than other nuclei such as ^{1}H, are well established, in particular the absence of magnetic couplings between the ^{13}C nuclei and the larger range of chemical shifts. This yields high resolution, easily interpretable spectra even for large molecules with many carbon nuclei. In contrast, the usefulness of ^{13}C NMR in solids to date has not been outstanding. In particular, this is due to extremely poor resolution and sensitivity. Despite the early realization that a great deal of information is potentially hidden in solid state spectra, it is only recently that such spectra have begun to emerge.

The quantity of prime interest at this stage is the chemical shielding tensor, of which only the trace is determined in liquid studies.[1,2] An expectation of both theoreticians and experimentalists approaching these problems is that studies of these tensors will aid in understanding magnetic shielding of nuclei and in obtaining orientational and structural information which is available only with difficulty or unavailable otherwise.

Several approaches have been taken to extracting high resolution ^{13}C NMR spectra from solids. All of them encounter the same problem, namely that of dipolar broadening by ^{1}H spins normally present, except in special isolated cases.[3,4] In one approach, the dipolar broadening is reduced by substituting ^{2}H for ^{1}H.[5] The latter has a much smaller magnetogyric ratio, but still leaves a problematic amount of broadening and will not yield very well resolved ^{13}C spectra for complex systems. This can be overcome by selective enrichment of ^{13}C, but introduces formidable and expensive preparative difficulties for general single crystal applications. Another approach employed by Schaefer and co-workers[6] involves rapid rotation of samples at the "magic angle," reducing the dipolar broadening.[7] However, this also removes the chemical shielding anisotropy of ^{13}C, leaving only the trace of the tensors observable.

The most promising approach appears to be that of ^{1}H–^{13}C nuclear magnetic double resonance, introduced recently in several versions.[8–10] We have found the approach of direct detection with sensitivity enhancement offered by proton-enhanced nuclear induction spectroscopy[8] to be most convenient and widely applicable. Using this approach, we have determined several ^{13}C tensors in molecules with carbon–oxygen bonds and from these data a picture of trends for particular functional groups is beginning to emerge. In this paper, we report details of the work in single crystals of ammonium D-tartrate. This material was selected because of several appealing features:

(a) large single crystals can be grown with facility;

(b) the crystal structure is known;

(c) it contains two functional groups of interest, C–OH and COO^-, for which full tensors have not been determined previously;

(d) the spectra and analysis are complex enough to indicate the types of problems encountered in those experiments;

(e) the analysis indicates a favorable case where the shielding tensors are related to the local symmetry at the ^{13}C sites.

In Sec. II a brief reminder of the basis for the double resonance approach is presented and in Sec. III details of the experimental apparatus and analysis are described. Results are presented for work on single crystals in Sec. IV, where the shielding values and orientational data are discussed and an indication of experimental

precision is given.

II. CARBON-13–PROTON DOUBLE RESONANCE

In this section we describe briefly the approach employed and some sensitivity considerations. Detailed discussions of sensitivity enhancement in double resonance experiments have been provided by several authors.[8–13] There are basically two difficulties with the extraction of high resolution ^{13}C NMR spectra from solid samples, sensitivity and resolution. The problem of sensitivity is a perennial one and is encountered also in normal ^{13}C NMR in liquids. In the case of solids, the problem is even more acute since resolution is lower, more lines are found, and spin–lattice relaxation times are normally long. The loss in resolution comes about primarily owing to magnetic dipolar coupling of the ^{13}C nuclei to abundant ^{1}H nuclei usually present in the sample. For these reasons, until recently, cases of resolved solid state ^{13}C spectra were reported employing conventional techniques only on samples devoid of protons.

The double resonance techniques are based on concepts originally introduced by Bloch[14] and Hahn and coworkers,[11] and have alleviated these problems to a large extent. Sensitivity enhancement is effected in the "cross polarization" step by transferring nuclear magnetic polarization from abundant (I) to the rare (S) spins. Subsequently, the resolution is enhanced by intense irradiation of the I nuclei at resonance, inducing spin decoupling during the observation of the S spin free precession. This process can be repeated until the I polarization is depleted, resulting in a large sensitivity enhancement over conventional Fourier transform spectroscopy.

To review briefly the considerations of sensitivity enhancement we consider two limiting versions of the experiment depicted in Fig. 1. The first is the approach we have employed most commonly, referred to as multiple cross polarization. In this approach, the I spins, after reaching equilibrium in the magnetic field with a magnetization $M_I^{(0)}$ are spin locked at resonance with an intense field of intensity H_{1I}. The cross polarization is effected by irradiating the S spins with a field H_{1s} such that the Hartmann–Hahn condition

$$\gamma_I H_{1I} = \gamma_s H_{1s} \tag{1}$$

is satisfied; cross relaxation is most efficient under these conditions. The S spin magnetization after this cross polarization step is given by

$$M_s^{(1)} = (\gamma_I/\gamma_s) M_s^{(0)}, \tag{2}$$

where $M_s^{(0)}$ is the magnetization with the S spins in equilibrium with the lattice. The S spin free induction decay is now observed while the irradiation of the I spin continues and the whole process can be continued with the S signal accumulated and ultimately Fourier transformed. The optimal number N of cross polarization steps depends on $T_{1\rho}$, the spin–lattice relaxation time of the I spins in the rotating frame. For the simple case $T_{1\rho} \to \infty$, the optimal enhancement in signal/noise voltage is realized for $N\sqrt{N_s/N_I} \approx 1$ for which

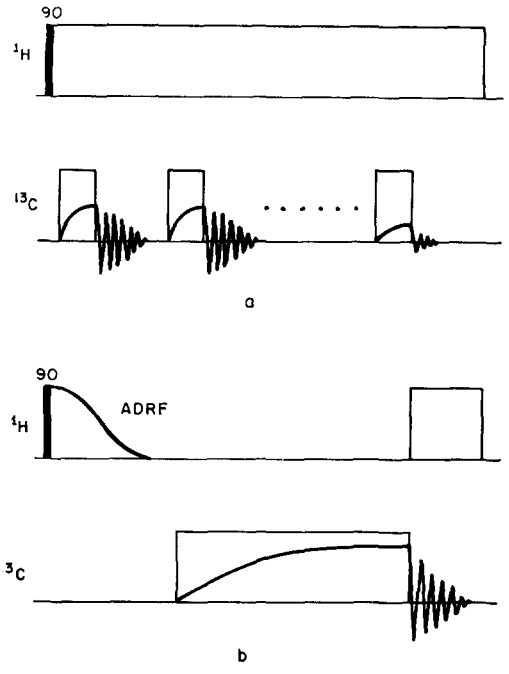

FIG. 1. Schemes for multiple cross polarization and single total cross-polarization versions of double resonance. (a) In this version the Hartmann–Hahn condition is matched and the ^{1}H polarization is transferred in steps to the ^{13}C nuclei, the ^{13}C free precession signal being accumulated during ^{1}H irradiation. (b) Here the ^{13}C nuclei are polarized with a large H_1 field from the ^{1}H system after adiabatic demagnetization in the rotating frame. This yields larger ^{13}C polarizations in one step but the cross-polarization times are longer.

$$\left(\frac{S}{N}\right)_{MCP} \approx 0.6 \frac{\gamma_I}{\gamma_s}\sqrt{\frac{N_I}{N_s}}\left(\frac{S}{N}\right)^{(0)}, \tag{3}$$

where N_I, N_s are the numbers of I and S spins and $(S/N)^{(0)}$ is the voltage signal/noise for a normal ^{13}C free induction decay.

The advantages of this approach are its simplicity and the fact that the number of contacts can be adjusted optimally for $T_{1\rho}$. The main disadvantage in the case of long $T_{1\rho}$ is that in order to realize the full sensitivity enhancement, prolonged irradiation of the I spins is necessary (for N cross polarization and accumulation steps) and the problem of power dissipation becomes acute. For many cases, however, a single cross polarization with the enhancement of Eq. (2) suffices and does not introduce severe problems of power dissipation.

The second limiting case, depicted schematically in Fig. 1 (b) is the one we have referred to as "total cross-polarization."[8,15,16] Here, by applying large H_{1s} fields, most or all of the ^{1}H polarization can be transferred to the S spins in one step. However, since the Hartmann–Hahn condition is not satisfied in this case, the cross relaxation is slow so that this is not always a profitable venture. The simplest version is that shown in the figure. Here, the ^{1}H system is first adiabatically demagnetized in the rotating frame and the ^{13}C nuclei are then polarized by turning on a strong radio-frequency field near resonance. The ^{13}C polarization achievable is

$$M_s^{(1)} = \alpha\,(\gamma_I/\gamma_s)\sqrt{N_I/N_s}\;M_s^{(0)}, \tag{4}$$

where $\alpha = 1$ if the ^{13}C field is turned on adiabatically and $\alpha = \frac{1}{2}$ is it is turned on suddenly.

For cases where spin–lattice relaxation times are long and it is desirable to realize the full sensitivity enhancement, then this approach is useful as long as T_{IS} does not become excessively long, since the full experimental time involves one cross polarization and one observation. Pines and Shattuck[15] have shown that $T_{IS} \sim 1$ sec for H_{1s} fields yielding large polarizations (x 15 in adamantane even with $T_{1d} \sim 100$ msec) and thus this approach can be profitable.

For the present experiments, several approaches were investigated. Since $T_{1\rho}$ and T_{1d} for the ^1H spins were found to be short, the multiple cross polarization was used with a small number of cross-polarization steps, normally one.

III. EXPERIMENTAL

Since this paper describes in detail the first in a series of experiments using our spectrometer on carbon-13 NMR in single crystals, we present more details on the experimental procedure and on the equipment required for the experiments. In addition, this section presents some details of the analysis employed to extract the chemical shielding tensors and assign them to molecules and bond directions. In general, our experimental procedure consists of the following steps:

(a) Mount the crystal in a well-machined reorientable cube with assigned axes (X_c, Y_c, Z_c).

(b) Orient the crystal employing x-ray techniques. This gives the crystallographic axes (a, b, c) relative to the cube axes (X_c, Y_c, Z_c).

(c) Obtain NMR spectra for orientations of the crystal about (X_c, Y_c, Z_c) perpendicular to H_0.

(d) Analyze the rotation plots to obtain the shielding tensors σ_c in the cube axes.

(e) Diagonalize σ_c, yielding σ in the principal axes system $(1, 2, 3)$. This gives the eigenvalues σ_{ii} and the orientation of $(1, 2, 3)$ relative to (X_c, Y_c, Z_c) and thus relative to (a, b, c).

(f) Assign the tensors σ to particular ^{13}C nuclei in the unit cell. This final step is not rigorous and involves some assumptions. However, this is the most interesting and valuable part of the experiment, particularly at this stage where so little is known about ^{13}C shielding tensors.

We describe in turn some details of the apparatus and analysis which permit the above procedure to be followed efficiently. This includes a description of the spectrometer, the probe and goniometer, sample orientation and data analysis.

A. Spectrometer

The spectrometer is a wideband double resonance device[17] which operates in heterodyne mode with an intermediate frequency of 30 MHz. A schematic diagram is shown

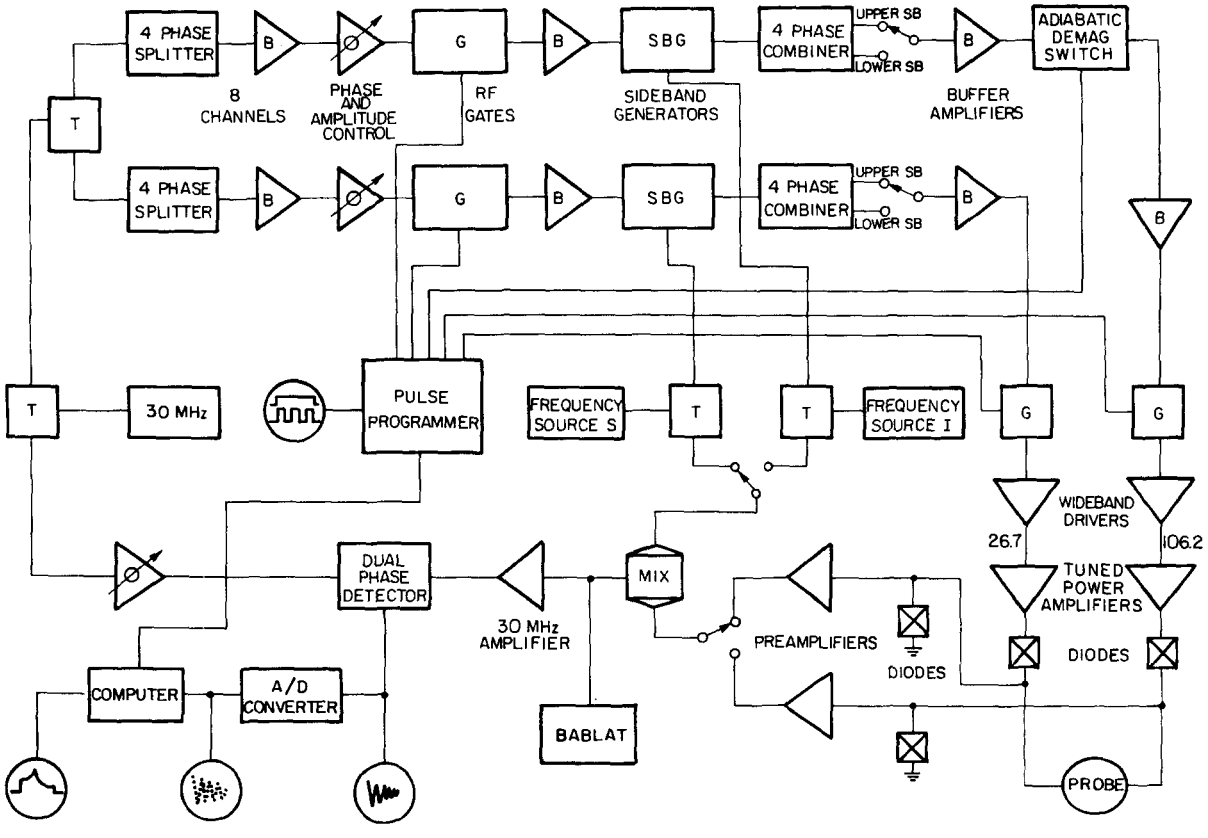

FIG. 2. Schematic diagram of double-resonance spectrometer.

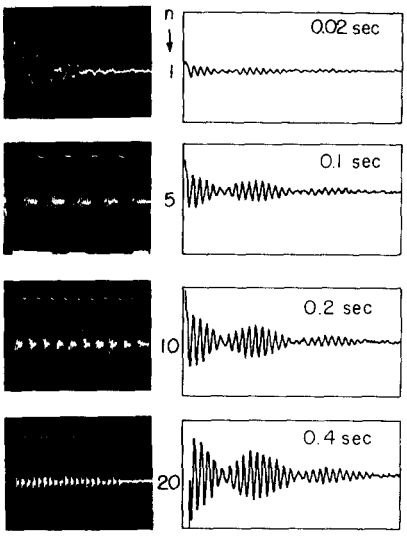

FIG. 3. Demonstration of sensitivity enhancement for carbon-13 spins. The oscillograph photographs on the left depict the output of the ^{13}C phase detector for various numbers (n) of $^{1}H \rightarrow {}^{13}C$ cross-polarization steps in solid adamantane. The positive pulses are from rf receiver blocking during the cross polarization, and they are followed by proton-decoupled ^{13}C free precession signals. It is these which are rapidly transferred and accumulated by the computer. The cross-polarization pulses are 5 msec long. The traces on the right show the accumulated signals and aquisition times corresponding to the number of cross-polarization steps on the left. These were recorded further away from resonance.

in Fig. 2. In principle, it is a double resonance version of the multiple-pulse spectrometer described elsewhere.[18] The magnet is a wide bore superconducting solenoid. The radio-frequency sections are mostly homebuilt from commercial hybrids, and the digital section is constructed around an on-line PDP 8/e minicomputer.

The low-level radio-frequency circuitry is separated from the power amplifiers to facilitate shielding of the detectors from the intense radiation. The transmitter section contains four phase channels for each frequency with phase and amplitude adjustments. Special features of the detector section are good shielding and isolation, high sensitivity, wideband operation, and flexibility. Frequency for the low level sections is selected by simply changing the source frequencies derived from synthesizers since all low level operation is wideband.

Power amplifiers are tuned and consist mainly of modified radio amateur transmitters. These are equipped with homebuilt power supplies designed for stable operation during the prolonged rf irradiation. The ^{1}H final stage, for example, is a modified Millen amplifier which operates in class C with a double glass tetrode. Anode voltage is 2000 V derived from a regulated power supply stable to 0.1%.

The digital section contains the minicomputer, pulse programmer, and a data aquisition system described briefly elsewhere.[19] The latter is exceedingly simple and employs the computer directly as a fast real time

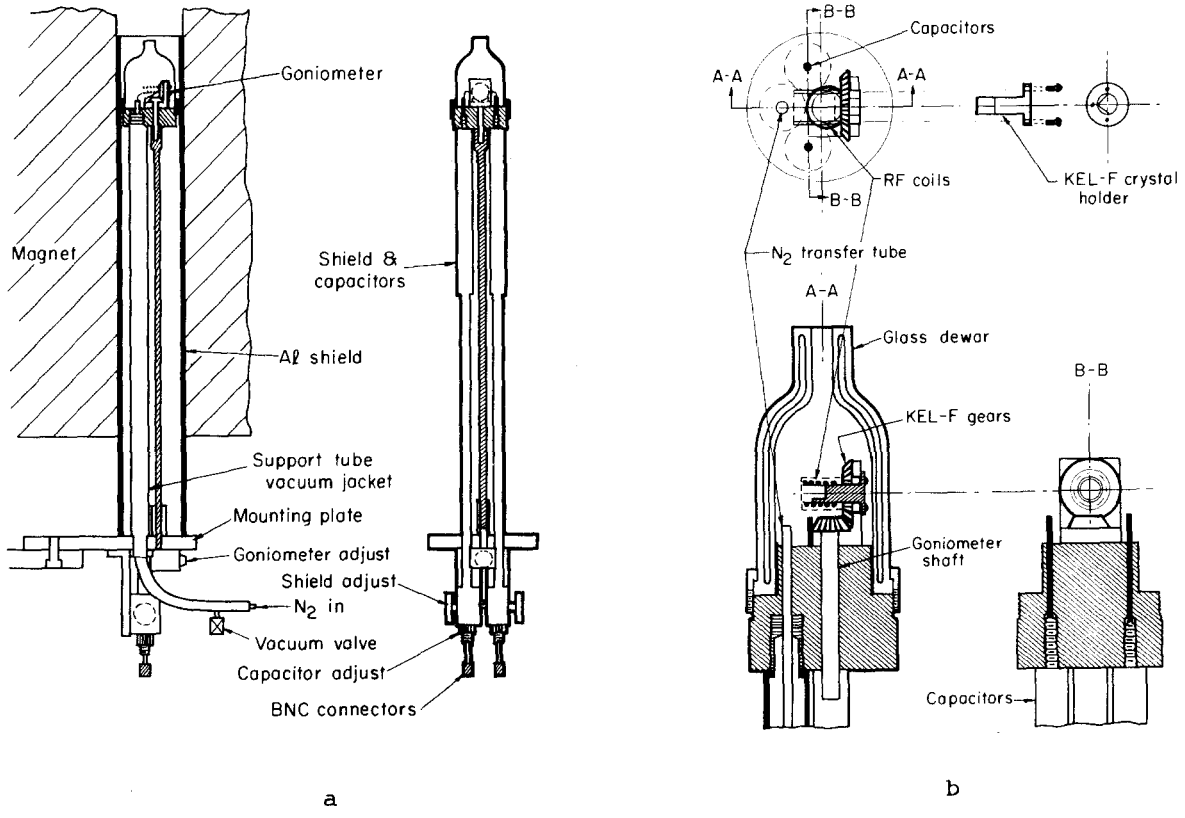

FIG. 4. Schematic diagram of double resonance probe and goniometer.

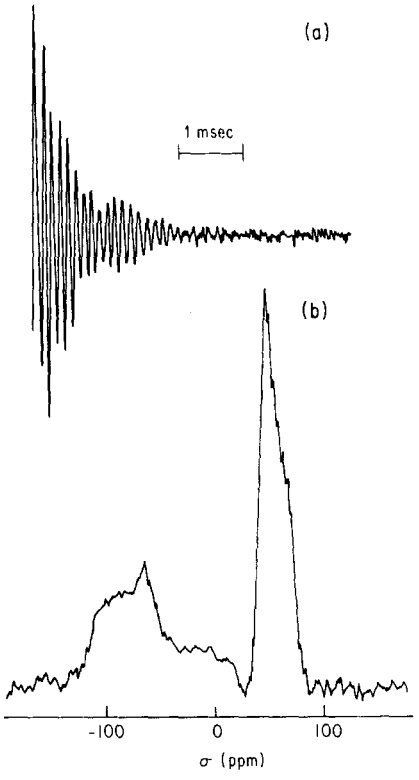

FIG. 5. Fourier transform proton-enhanced ^{13}C NMR spectrum in polycrystalline ammonium D-tartrate at 23 °C. The horizontal scale is in ppm-relative to an external reference of liquid benzene. The low field peak is from the carboxyl carbon nuclei and the high field from hydroxyl carbon nuclei; both display an anisotropy of the chemical shift. Values for the principal elements of the shielding tensors extracted from this spectrum appear in Table I.

signal averager through the "direct add to memory" option. The pulse programmer is a homebuilt device controlled by the computer. It operates asynchronously with an independent memory and with facilities to control 16 pulse channels and 2 channels for adiabatic demagnetization and remagnetization. The computer handles pulse programming, data aquisition, data storage and filing, display, data analysis, etc.

An example of the sensitivity enhancement provided by the spectrometer is given in Fig. 3. This provides a demonstration of the accumulative cross polarization processes for ^1H–^{13}C double resonance in a polycrystalline sample of adamantane. For the present experiments on ammonium D-tartrate, good signal/noise was obtained by averaging over several ^1H polarization cycles, typically in less than 5 min per spectrum.

B. Probe and Goniometer

Figure 4 shows a schematic diagram of the probe employed for the geometry of the superconducting solenoid, with details of the probe head containing the variable temperature sample chamber, radio-frequency coils, and goniometer. The ^{13}C coil is a short horizontal solenoid of diameter 6 mm and the ^1H coils are wound orthogonal in a Helmholtz configuration. The double coil is mounted on leads supported in a Kel-F base and connected to rigid coaxial cable via shielded tuning and matching circuits.

The goniometer consists of precision Kel-F gears with a shaft that can be rotated remotely. The lower end of the shaft is connected to a gear and calibrated dial permitting the angle of the upper gear to be read directly. The crystal holder is shown in the detail of Fig. 4(b) and is keyed onto the vertical gear so that its position and orientation are precisely reproducible. The cube containing the crystal is cemented onto the end of the crystal holder and is positioned in the center of the coils when the holder is keyed in position and fixed with the set screws.

The tuning and matching electronics consist primarily of homebuilt capacitors to withstand the high radio-frequency voltages across the coils. These are housed beneath the Kel-F base in shielded tubes and consist of polished smooth copper tubes with Teflon dielectric. The capacitance is adjustable remotely as shown in the figure to permit tuning with the probe in position inside the magnet bore.

C. Sample Orientation

Crystals of ammonium D-tartrate were grown from aqueous solution by slow evaporation. The crystals were mounted in Kel-F cubes machined to match a crystal holder as shown in Fig. 4(b). The cubes holding the crystals are assigned axes (X_c, Y_c, Z_c). The crystal holders were keyed onto the end of an x-ray goniometer, maintaining the orientation of the crystal between the NMR goniometer and the x-ray equipment.

The crystal structure of ammonium D-tartrate has been determined previously[20]: space group $P2_1$, with two molecules in the unit cell. The crystallographic a, b, c axes were located in an x-ray precession experiment, and the orientations of (X_c, Y_c, Z_c) relative to the orthogonal system (a, b, c^*) were then determined directly.

D. Rotation Plots and Data Analysis

The chemical shift σ is related to the zz component of the shielding tensor in the laboratory frame, where z is the direction of the magnetic field. For a rotation about the axis k of the crystal cube, it is easily shown that[21]

$$\sigma = \tfrac{1}{2}(\sigma_{ii} + \sigma_{jj}) - \tfrac{1}{2}(\sigma_{ij} + \sigma_{ji}) \sin 2\theta + \tfrac{1}{2}(\sigma_{ii} - \sigma_{jj}) \cos 2\theta , \quad (5)$$

where $\{i, j, k\} \equiv \{X_c, Y_c, Z_c\}$ with cyclic permutations.

The coefficients containing the elements of σ are determined for each rotation by fitting the rotation data to

TABLE I. Elements of σ in ammonium D-tartrate from powder spectrum (in ppm) relative to external reference of liquid benzene.[a]

	σ_{11}	σ_{22}	σ_{33}
$^{13}COO^-$	−116.0	−70.0	15.5
^{13}COH	39.2	39.2	72.1

[a]Error range is ±6 ppm.

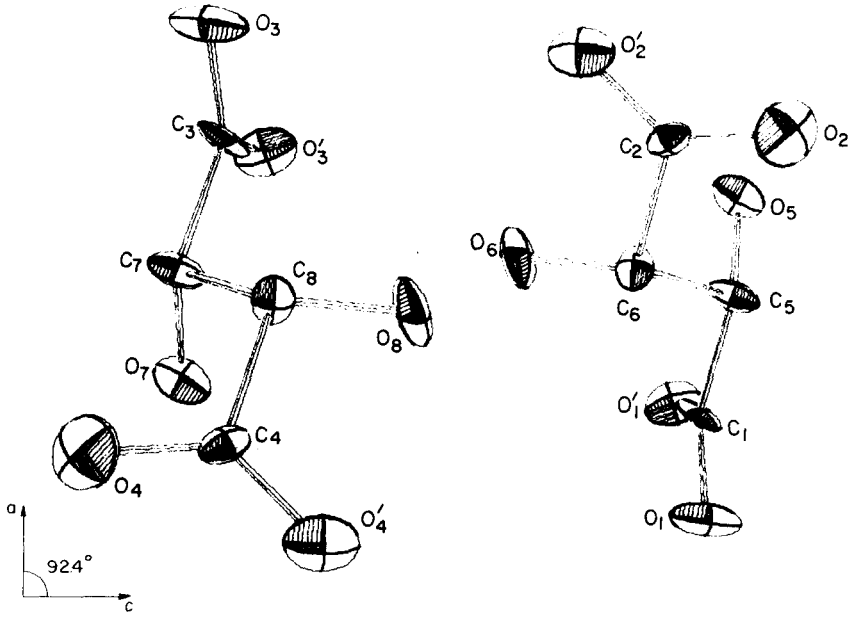

FIG. 6. Perspective view along the crystallographic b axis of two tartrate ions, showing the carbon and oxygen atoms in the unit cell of ammonium D-tartrate. The labeling of the atoms corresponds to that used in the discussion of tensor orientations relative to molecular bond directions.

Eq. (5) and from the three rotations, nine equations are obtained for the six parameters of the shielding tensor; the latter are extracted by least squares fitting. At this stage the shielding tensor elements (the symmetric part) in the cube axes are fully determined. This is now diagonalized by standard procedures to yield the principal values σ_{ii} and the orientation of the principal axes of σ in the cube axis system.

IV. RESULTS

As indicated previously, three independent sets of measurements were performed on two different crystals. Results are presented here for the three determinations to give an idea of the experimental precision available at this preliminary stage of the development of our apparatus and procedure. Several sources of error contribute towards the small fluctuations in results, including x-ray orientation, goniometer misalignment, errors in cube reorientation, and spectral resolution. We describe first the limited results of a powder spectrum and then provide details on spectra from crystals, orientation plots, and determination of the tensors.

A. Powder Spectrum

Powder spectra are simple to obtain by our method and in favorable cases can yield directly the principal elements of the chemical shielding tensors.[22] Clearly, the orientational information is normally lost. In cases where there is severe overlap between lines, analyzing the spectrum is not a trivial problem; it can be approached by several methods aside from full single crystal studies, including partial cross relaxation, selective ^{13}C enrichment, and detailed line shape analysis.

Figure 5 shows the ^{13}C proton-enhanced free induction decay and Fourier transform NMR spectrum obtained from a polycrystalline sample of ammonium D-tartrate. In this case, the assignment is simple, the two peaks arising from the carboxyl and hydroxyl carbon nuclei. The principal values of the shielding tensors extracted directly from this spectrum are given in Table I and are compared later with values obtained from the single crystal work. Note that within experimental error the shielding tensor for the ^{13}C–OH groups is axially symmetric.

B. Single Crystal Spectra

The unit cell of ammonium D-tartrate contains two molecules, as shown in Fig. 6. In isotropic liquid solu-

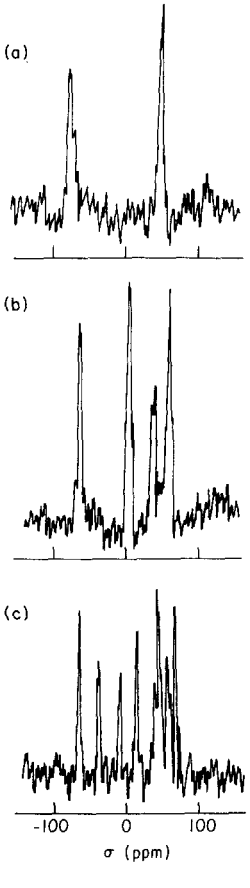

FIG. 7. Fourier transform proton-enhanced ^{13}C NMR spectra of the single crystal of ammonium D-tartrate in three different orientations. The horizontal scale is relative to an external reference of liquid benzene.

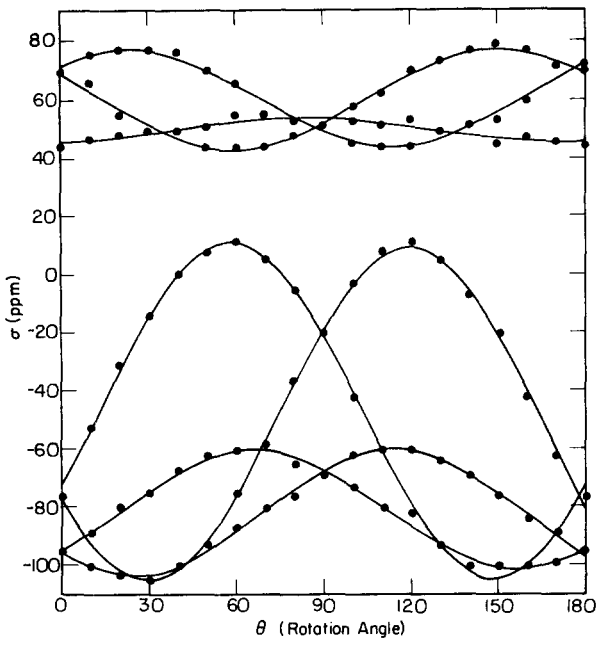

FIG. 8. Dependence of line positions in ^{13}C spectra of ammonium D-tartrate on crystal orientation about the crystallographic a axis.

tion only two lines are observed from the magnetically inequivalent carboxyl and hydroxyl nuclei. In the crystal, all eight carbon nuclei can be magnetically inequivalent and we expect to see several lines. Figure 7 shows proton-enhanced ^{13}C spectra from a single crystal of ammonium D-tartrate in different orientations, displaying the resolution of lines from all the nuclei in the unit cell. The resolution is limited primarily by magnetic field inhomogeneity and by dipolar coupling to ^{14}N spins.

C. Orientation Dependence

As explained in Sec. III a full analysis of the data is performed by taking spectra such as those in Fig. 7 for rotations about the cube axes (X_c, Y_c, Z_c). The orientation dependence of the line position for such a rotation on one of the crystals is given in Fig. 8. Similar data are obtained from the other determinations. The relevant information is provided in the caption. The data are fitted to Eq. (5), and the tensors in the cube axes are then determined by combining sets of lines from the three rotations. The sets of lines are easily assigned in this case by the requirement that they match up at equivalent orientations of the cube and by the requirement that they provide "reasonable" tensors (see following discussion). Owing to problems of resolution and line assignment for the hydroxyl lines, the errors are much larger as manifested later in the orientation determination.

D. Shielding Tensors

Since there are eight inequivalent carbon nuclei in the unit cell (see Fig. 6), we expect to obtain eight different shielding tensors from the analysis. Employing the data from x-ray crystal orientation work, the principal axes are then known with respect to the crystallographic axes. This part of the analysis is rigorous and involves no assumptions. In the next section, assumptions are made to relate σ to the molecules, since clearly the tensors can be assigned in several ways to specific ^{13}C nuclei, subject only to the constraint that they must conform to the transformations of the crystallographic symmetry.

The shielding values are shown in Table II for the four $^{13}COO^-$ and four ^{13}COH tensors determined by diagonalization of the tensors in the cube axis system. As men-

TABLE II. Elements of σ from single crystal work (in ppm relative to external reference of liquid benzene).

		Tensor 1	Tensor 2	Tensor 3	Tensor 4	Average
		−110.1	−107.4	−110.8	−109.6	
	σ_{11}	−111.2	−105.1	−109.4	−109.4	−110.5
		−115.8	−114.4	−112.0	−110.2	
		−66.4	−57.8	−62.2	−56.5	
$^{13}COO^-$	σ_{22}	−63.7	−58.7	−63.4	−56.3	−61.7
		−68.1	−61.6	−65.3	−59.8	
		26.2	20.2	23.3	22.1	
	σ_{33}	22.7	19.9	21.8	21.7	21.6
		22.5	18.9	18.2	21.2	
		Tensor 5	Tensor 6	Tensor 7	Tensor 8	
		46.0	42.6	41.5	44.0	
	σ_{11}	41.2	43.8	42.7	42.4	41.9
		39.9	40.9	39.0	39.0	
		49.7	49.5	50.6	45.9	
^{13}COH	σ_{22}	49.7	46.2	49.9	47.9	48.0
		46.8	47.2	46.8	45.4	
		75.9	74.8	77.7	76.0	
	σ_{33}	76.0	74.3	74.7	73.7	74.0
		70.9	70.1	72.8	70.7	

TABLE III. Direction cosines of principal axes of tensors relative to crystallographic axes.

		a	*b*	*c**	*a*	*b*	*c**	*a*	*b*	*c**	*a*	*b*	*c**
		Tensor 1			Tensor 2			Tensor 3			Tensor 4		
$^{13}COO^-$	σ_{11}	−0.8062	−0.5305	−0.2618	0.7996	0.5840	0.1399	0.8671	−0.3776	0.3249	−0.8833	0.4528	−0.3185
		−0.8099	−0.4883	−0.3250	0.8164	0.5312	0.2266	0.8399	−0.4359	0.3235	−0.7863	0.5383	−0.3031
		−0.8281	−0.4658	−0.3120	0.8045	0.5348	0.2585	0.8766	−0.4206	0.2349	−0.8254	0.5271	−0.2025
	σ_{22}	0.5653	−0.8213	−0.0768	−0.4005	0.3448	0.8500	−0.4446	−0.8806	0.1632	0.4385	0.1882	−0.8788
		0.5488	−0.8264	−0.1258	−0.4133	0.2631	0.8719	−0.4871	−0.8683	0.0947	0.4752	0.2135	−0.8536
		0.5398	−0.8129	−0.2191	−0.4277	0.2198	0.8768	−0.4509	−0.8875	0.0950	0.4014	0.2955	−0.8670
	σ_{33}	0.1743	0.2099	−0.9620	−0.4477	0.7349	−0.5094	−0.2246	0.2860	0.9317	0.3380	0.8716	0.3552
		0.2072	0.2802	−0.9373	−0.4036	0.8053	−0.4342	−0.2396	0.2371	0.9415	0.3947	0.8152	0.4238
		0.1516	0.3498	−0.9244	−0.4121	0.8159	−0.4055	−0.1670	0.1885	0.9678	0.3971	0.7968	0.4554
		Tensor 5			Tensor 6			Tensor 7			Tensor 8		
^{13}COH	σ_{11}	0.4357	0.8395	−0.3247	−0.8458	−0.4646	0.2625	−0.5170	0.8447	0.1384	0.9807	−0.1372	−0.1393
		0.4689	0.8794	−0.0818	−0.9928	−0.0925	0.0758	−0.4237	0.9014	0.0891	0.8663	−0.4354	−0.2448
		0.4860	0.8722	−0.0547	−0.9964	−0.0050	0.0854	−0.4635	0.8837	0.0645	0.8094	−0.5081	−0.2943
	σ_{22}	−0.1578	0.4264	0.8907	−0.5336	0.7387	−0.4118	0.0621	0.1982	−0.9782	0.1768	0.9267	0.3318
		−0.1358	0.1633	0.9772	−0.1165	0.8908	−0.4394	0.1123	0.1500	−0.9823	0.4994	0.7658	0.4051
		−0.0888	0.1149	0.9898	−0.0355	0.9320	−0.3608	0.1058	0.1274	−0.9861	0.5871	0.7107	0.3877
	σ_{33}	0.8862	−0.3368	0.3182	−0.0026	−0.4884	−0.8776	−0.8539	−0.4971	−0.1550	0.0836	−0.3501	0.9330
		0.8728	−0.4471	0.1959	−0.0269	−0.4451	−0.8951	−0.8989	−0.4062	−0.1648	0.0111	−0.4732	0.8808
		0.8695	−0.4762	0.1316	−0.0778	−0.3625	−0.9288	−0.8797	−0.4503	−0.1526	0.0122	−0.4866	0.8736

tioned previously, three independent experiments were performed, one experiment on one crystal and two on a second crystal. The three entries are for these three determinations, and the average indicates an average over all 12 values for the four tensors and three determinations. It is hard to attach any significance to the difference between the tensors from similar carbon nuclei, since they appear to be in the range of experimental error. The precision is good (±2 ppm) and the values are in agreement with the determination from the powder spectrum (Fig. 5, Table I) within experimental error.

Of particular interest is the orientation of the principal axes of σ. This is summarized in Table III for the three determinations, as direction cosines of (1, 2, 3) relative (a, b, c^*), for each of the eight tensors.

E. Assignment to Specific ^{13}C Nuclei

The only rigorous orientational output of our experiment is the orientation of σ in the crystallographic axes. However, one of the reasons for undertaking this whole project is to see if σ is related to local structure and symmetry. For an isolated COO^- group with equal C–O bonds we expect one axis of σ to be perpendicular to the plane, one to bisect the CO bonds, and the third to be perpendicular to these two. For an isolated CH_3O group analogous to the hydroxyl carbon, we expect a unique axis along the CO bond and two others degenerate and perpendicular. Indeed, one assignment of tensors to carbon nuclei conforms quite closely to these require-

TABLE IV. Orientation of principal axes of ^{13}C shielding tensors relative to molecular bond directions.[a]

		Tensor 1			Tensor 2			Tensor 3			Tensor 4		
	Bond	$C_5-{}^{13}C_1$[b]	$\parallel(^{13}COO)_1$[c]	$\perp(^{13}COO)_1$[d]	$C_6-{}^{13}C_2$	$\parallel(^{13}COO)_2$	$\perp(^{13}COO)_2$	$C_7-{}^{13}C_3$	$\parallel(^{13}COO)_3$	$\perp(^{13}COO)_3$	$C_8-{}^{13}C_4$	$\parallel(^{13}COO)_4$	$\perp(^{13}COO)_4$
		3.2	86.9	87.9	7.2	86.1	89.8	7.9	95.7	82.9	5.7	86.9	100.5
	σ_{11}	4.7	88.6	83.9	1.3	90.4	94.5	5.3	92.1	83.5	4.4	85.7	95.1
		3.9	90.4	84.5	1.9	88.4	94.7	4.3	94.5	88.5	2.3	91.9	94.5
		93.1	3.6	92.0	87.0	8.8	81.7	84.4	5.7	88.8	93.0	3.4	88.3
$^{13}COO^-$	σ_{22}	91.4	1.6	89.4	89.7	4.5	85.5	87.8	3.1	92.1	94.4	6.0	85.5
		90.1	5.8	84.2	91.6	3.2	87.1	85.5	5.3	92.6	88.3	6.2	84.3
		90.6	88.1	2.9	96.5	98.3	8.3	95.6	90.5	7.1	85.2	91.2	10.7
	σ_{33}	94.5	90.7	6.1	91.3	94.6	6.4	94.8	87.6	6.8	90.5	94.1	6.8
		93.9	95.8	8.1	91.0	92.8	5.6	89.6	87.3	2.9	91.6	95.9	7.3
		Tensor 5			Tensor 6			Tensor 7			Tensor 8		
	Bond	$^{13}C_5-O_5$[e]	$^{13}C_5-C_1$	$^{13}C_5-C_6$	$^{13}C_6-O_6$	$^{13}C_6-C_2$	$C_5-{}^{13}C_6$	$^{13}C_7-O_7$	$^{13}C_7-C_3$	$^{13}C_7-C_8$	$^{13}C_8-O_8$	$^{13}C_8-C_7$	$C_4-{}^{13}C_8$
		103.0	133.9	26.6	96.0	150.7	132.7	98.6	144.2	38.3	99.5	147.6	113.3
	σ_{11}	101.7	143.3	40.6	97.5	147.9	108.8	104.6	140.6	39.6	96.0	151.4	130.5
		100.6	145.0	42.3	100.4	143.4	105.7	102.1	143.4	41.5	96.2	149.0	136.3
		108.3	145.3	107.2	92.5	99.1	46.9	95.0	106.7	123.8	99.3	75.5	33.7
^{13}COH	σ_{22}	97.0	132.6	102.0	92.6	75.2	26.2	95.5	102.8	127.1	93.3	96.6	45.2
		93.8	103.0	129.0	87.1	68.7	27.8	94.4	102.6	128.3	93.3	102.2	50.5
		22.7	131.0	105.6	6.5	117.6	74.4	10.0	120.7	105.8	13.4	118.2	67.0
	σ_{33}	13.7	124.3	105.2	8.0	117.8	71.9	15.7	126.5	102.0	6.9	117.7	73.5
		11.0	121.9	103.8	12.7	118.3	67.7	12.8	123.7	103.5	7.0	118.0	74.4

[a] The numbering of the atoms corresponds to that in Fig. 7. The three entries are from the three independent determinations.
[b] $C_i-{}^{13}C_j$ is along the $C_i-{}^{13}C_j$ bond bisecting the $^{13}C_jO_j$ bonds.
[c] $\parallel(^{13}COO)_j$ is in the $^{13}C_jO_jO'_j$ plane perpendicular to the $C_i-{}^{13}C_j$ bond
[d] $\perp(^{13}COO)_j$ is perpendicular to the $^{13}C_jO_jO'_j$ plane.
[e] $^{13}C_j-O_j$ is along the hydroxyl carbon $^{13}C_j-O_j$ bond.

ments. Our assumption that this is the correct assignment is strengthened by other experiments in which one assignment yields the heaviest shielding for $^{13}COO^-$ when H_0 is perpendicular to the plane.[23,24] The orientations are summarized in Table IV as angles between the principal axes of the tensors and bonds to the ^{13}C to which they are assigned.

We see that with this assignment σ conforms reasonably well to the local symmetry with σ_{33} (COO^-) being perpendicular to the COO^- plane and σ_{33} (COH) being along the CO bond. The orientation for the $^{13}COO^-$ group is summarized in Fig. 9.

F. Comments

The shielding values and orientation of the tensors for the carboxyl groups are determined quite precisely in this study, with a reproducibility of ± 2 ppm and ± 3° between the three determinations. The data for the hydroxyl groups are less satisfactory because of the limited resolution among the lines but are still instructive as far as the main features of the tensors are concerned. The determinations could be made considerably more precise by employing higher proton decoupling fields and a more uniform dc magnetic field.

Based on these results and others determined in our laboratory, several comments can be made in summary. For carboxyl groups the most shielded element (σ_{33}) of the ^{13}C tensor corresponds to an axis perpendicular to the $^{13}COO^-$ plane. For the carbonyl carbon in benzophenone, σ_{33} was also found to be perpendicular to the nodal plane of the CO II molecular orbital.[5] The orientations of the other two axes of the tensor depend on structure. It is interesting to observe the trend in orientation of the tensor as we proceed from the case of a symmetrical ketone to a symmetrical carboxyl group. This is depicted in Fig. 10 from results on benzophenone,[5] dimethyl oxalate,[23] and other work on carboxyl groups in our laboratory. Since the difference between (c) and (d) derives from the effects of hydrogen bonding, we feel that ^{13}C shielding tensors will provide a sensitive tool for the study of such bonding.

The shielding values for the hydroxyl carbon are in agreement with those determined for methanol;[25] thus, they appear to be characteristic for this type of functional group. The tensor conforms to the local symmetry of an isolated R_3CO group with the heaviest shielding along the CO bond.

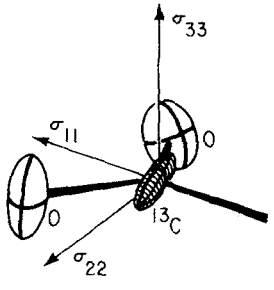

FIG. 9. Orientation of principal axes of ^{13}C chemical shielding tensor in carboxyl groups of ammonium D-tartrate. The ^{13}C nucleus is most shielded when H_0 is perpendicular to the $^{13}COO^-$ plane and least shielded when H_0 is along the C–^{13}C bond bisecting the ^{13}CO bonds.

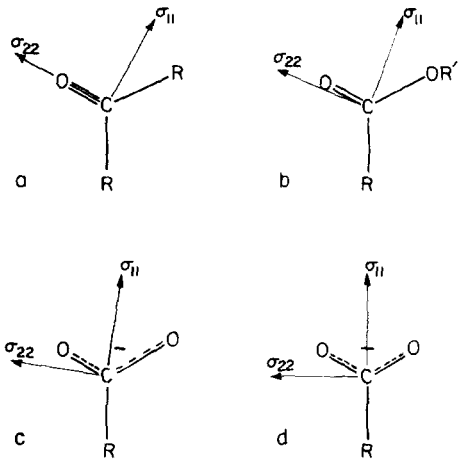

FIG. 10. Trends in the orientation of the principal axes of the ^{13}C chemical shielding tensor for various carbonyl groups. The most shielded axis, corresponding to σ_{33}, is perpendicular to the planes of the groups shown. As we proceed from the symmetrical ketone (a) through an ester group (b), an unsymmetrical (c) and a symmetrical (d) carboxyl group, axes 1 and 2 rotate systematically in the plane. The cases (a)–(d) are exemplified, respectively, by benzophenone, dimethyl oxalate, malonates, and the diammonium salts of oxalic and tartaric acids.

ACKNOWLEDGMENTS

We are indebted to D. D. Wilkinson and D. N. Shirley for extensive assistance with the equipment and computer programs and to Dr. A. Zalkin and Dr. G. Chapuis for assistance with the x-ray precession work. A. P. is particularly grateful to Professor D. H. Templeton for some valuable conversations on shielding tensors and crystal structure. Financial support from the National Science Foundation, Research Corporation, and the U.S. Atomic Energy Commission through the Inorganic Materials Research Division of the Lawrence Berkeley Laboratory is gratefully acknowledged.

*Supported in part by a Cottrell Research Grant from Research Corp. and in part by the National Science Foundation.

†Visitor of the Inorganic Materials Research Division. Permanent address: Francis Bitter National Magnet Laboratory, Cambridge, MA 02139.

[1] J. B. Stothers, *Carbon-13 NMR Spectroscopy* (Academic, New York, 1972); George C. Levy and Gordon L. Nelson, *Carbon-13 Nuclear Magnetic Resonance for Organic Chemists* (Wiley-Interscience, New York, 1972).

[2] N. F. Ramsey, Phys. Rev. 78, 699 (1950); J. W. Emsley, P. Feeney, and L. H. Sutcliffe, *High Resolution NMR Spectroscopy* (Pergamon, London, 1967); R. Ditchfield and P. D. Ellis, *Topics in Carbon-13 NMR* (Wiley-Interscience, New York, to be published), Vol. 1.

[3] P. C. Lauterbur, Phys. Rev. Lett. 1, 343 (1958).

[4] A. Pines, W. K. Rhim, and J. S. Waugh, J. Chem. Phys. 54, 5438 (1971).

[5] J. Kempf, H. W. Spiess, U. Haeberlen, and H. Zimmermann, Chem. Phys. Lett. 17, 39 (1972).

[6] J. Schaefer, presented at the Fourteenth Experimental NMR Conference, Boulder, CO, 1973.

[7] E. R. Andrew, in *Progress in Nuclear Magnetic Resonance Spectroscopy*, edited by J. W. Emsley, J. Feeney, and L. H. Sutcliffe (Pergamon, London, 1971), Vol. 8.

[8]A. Pines, M. G. Gibby, and J. S. Waugh, J. Chem. Phys. **56**, 1776 (1972); **59**, 569 (1973).
[9]H. E. Bleich and A. G. Redfield, J. Chem. Phys. **55**, 5405 (1971); C. S. Yannoni and H. E. Bleich, *ibid.* **55**, 5401 (1971).
[10]P. Mansfield and D. K. Grannell, J. Phys. C **1971**, L177.
[11]S. R. Hartmann and E. L. Hahn, Phys. Rev. **128**, 2042 (1962); D. A. McArthur, E. L. Hahn, and R. Walstedt, *ibid.* **188**, 609 (1969).
[12]E. P. Jones and S. R. Hartmann, Phys. Rev. B **6**, 757 (1972).
[13]F. M. Lurie and C. P. Slichter, Phys. Rev. **133**, A1108 (1964).
[14]F. Bloch, Phys. Rev. **111**, 841 (1958); L. R. Sarles and R. M. Cotts, *ibid.* **111**, 853 (1958).
[15]A. Pines and T. W. Shattuck, Chem. Phys. Lett. **23**, 614 (1973); A. Pines, in Proceedings of the First Specialized Colloque Ampère, Krakow, Poland, 1973 (to be published).
[16]A. Pines and T. W. Shattuck, J. Chem. Phys. **61**, 1255 (1974).
T. W. Shattuck, presented at the Philadelphia APS meeting, March 1974, Bull. Am. Phys. Soc. **19**, 351 (1974).
[17]A. Pines and D. D. Wilkinson (unpublished).
[18]J. D. Ellett, Jr., *et al.*, Adv. Magn. Reson. **5**, 117 (1971).
[19]T. Merrick, S. Smiriga, and A. Pines, J. Magn. Reson. (to be published).
[20]V. S. Yadova and V. M. Padnamabhan, Acta Cryst. B **29**, 493 (1973).
[21]M. Mehring, R. G. Griffin, and J. S. Waugh, J. Chem. Phys. **55**, 746 (1971).
[22]N. Bloembergen and T. J. Rowland, Phys. Rev. **97**, 1679 (1955); Acta Metall. **1**, 731 (1953).
[23]A. Pines and E. Abramson, J. Chem. Phys. (to be published).
[24]A. Pines, paper presented at the Fifteenth Experimental NMR Conference, Raleigh, NC, 1974.
[25]A. Pines, M. G. Gibby, and J. S. Waugh, Chem. Phys. Lett. **15**, 373 (1972).